International Journal of Non–Linear Mechanics 160 (2024) 104646

Contents lists available at ScienceDirect

International Journal of Non-Linear Mechanics

journal homepage: www.elsevier.com/locate/nlm

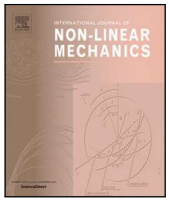

An extrapolation approach within the Wiener path integral technique for efficient stochastic response determination of nonlinear systems

Ilias G. Mavromatis [a], Ioannis A. Kougioumtzoglou [a,*], Pol D. Spanos [b]

[a] Department of Civil Engineering and Engineering Mechanics, Columbia University, 610 S.W. Mudd Building, 500 W. 120th St., New York, NY, 10027, USA
[b] L. B. Ryon Chair in Engineering, Rice University, 6100 Main, Houston, TX, 77005-1827, USA

ARTICLE INFO

Keywords:
Stochastic dynamics
Nonlinear system
Path integral
Boundary value problem
Most probable path

ABSTRACT

An extrapolation approach within the Wiener path integral (WPI) technique is developed for determining the stochastic response of diverse nonlinear dynamical systems. Specifically, the WPI technique treats the system response joint transition probability density function (PDF) as a functional integral over the space of all possible paths connecting the initial and the final states of the response vector. Further, the functional integral is evaluated, ordinarily, by considering the contribution only of the most probable path. This corresponds to an extremum of the functional integrand, and is determined by solving a functional minimization problem that takes the form of a deterministic boundary value problem (BVP). This BVP corresponds to a specific grid point of the response PDF domain. Remarkably, the BVPs corresponding to two neighboring grid points not only share the same equations, but also the boundary conditions differ only slightly. This unique aspect of the technique is exploited herein. Specifically, it is shown that solution of a BVP and determination of the response PDF value at a specific grid point can be used for extrapolating and estimating efficiently the PDF values at neighboring points without the need for considering additional BVPs. Notably, the herein developed approach enhances significantly the computational efficiency of the WPI technique without, practically, affecting the associated degree of accuracy. Two numerical examples relating to a Duffing nonlinear oscillator subjected to combined stochastic and deterministic periodic loading, and to an oscillator with asymmetric nonlinearities and fractional derivative elements are considered to demonstrate the reliability of the extrapolation approach. Juxtapositions with pertinent Monte Carlo simulation data are included as well.

1. Introduction

Several methodologies have been developed in the field of stochastic engineering dynamics over the last six decades, with varying degrees of success, for determining response and reliability statistics of structural and mechanical systems. The interested reader is directed to references such as the books by Lin [1], Nigam [2], Elishakoff [3], Ghanem and Spanos [4], and Lutes [5], for a broad perspective. More specifically, the available approximate/semi-analytical methodologies can be broadly divided into two groups. The first group comprises techniques that can treat accurately low probability events, but can handle only a small number of stochastic dimensions due to prohibitive associated computational cost. Representative examples include discrete versions of the Chapman–Kolmogorov equation (e.g., [6,7]), Fokker–Planck equation solution schemes (e.g., [8]) and probability density evolution methods (e.g., [9]). The second group comprises techniques, such as statistical linearization schemes (e.g., [10,11]), that can treat readily high-dimensional systems, but provide reliable estimates for low-order response statistics only, e.g., mean vector and covariance matrix.

Further, it can be argued that Monte Carlo simulation (MCS) is the most versatile numerical methodology for solving stochastic equations of arbitrary form (e.g., [12–14]). Note, however, that there are many cases where MCS can be computationally prohibitive. This is particularly true when high-dimensional complex systems are considered, for which even only one deterministic analysis is time-consuming. It is also true when the system response quantity of interest is characterized by a quite low probability of occurrence, with a computationally intractable number of deterministic analyses required to acquire a reasonably accurate estimate.

More recently, the Wiener path integral (WPI) technique was introduced in the field of stochastic engineering mechanics in [15–17]. Remarkably, the technique has been found to be both of high accuracy, and of low computational cost in a wide range of applications pertaining to diverse dynamical systems (e.g., [18–21]). Further, the

* Corresponding author.
E-mail address: ikougioum@columbia.edu (I.A. Kougioumtzoglou).

https://doi.org/10.1016/j.ijnonlinmec.2024.104646
Received 8 November 2023; Received in revised form 18 December 2023; Accepted 8 January 2024
Available online 11 January 2024

WPI technique has proven to be versatile in treating a wide range of nonlinear/hysteretic systems, even for those endowed with fractional derivative elements (e.g., [22–24]).

The fundamental concept of the WPI technique relates to treating the system response joint transition probability density function (PDF) as a functional integral over the space of all possible paths connecting the initial and the final states of the response vector. Further, the functional integral is evaluated, ordinarily, by resorting to an approximate approach that considers the contribution only of the most probable path. This corresponds to an extremum of the functional integrand, and is determined by solving a functional minimization problem that takes the form of a deterministic boundary value problem (BVP). This BVP corresponds to a specific grid point of the response PDF domain. Note, however, that for any particular nonlinear system under consideration, the equations of the BVP are independent of the grid point. In fact, only the boundary conditions change with different grid points, whereas the equations of the BVP remain unaltered. Remarkably, the BVPs corresponding to two neighboring grid points not only share the same equations, but also the boundary conditions differ only slightly. Thus, it is expected that the BVP solutions, i.e., the most probable paths, referring to the two grid points are highly correlated.

In this paper, the above unique aspect of the technique is explored further. Specifically, it is shown that solution of a BVP and determination of the response PDF value at a specific grid point can be used for extrapolating and estimating efficiently the PDF values at neighboring points without the need for solving additional BVPs. Notably, the herein developed approach enhances significantly the computational efficiency of the WPI technique without, practically, affecting the associated degree of accuracy. The latter is shown to be true even for relatively large distances between the original and the extrapolated points. Two numerical examples relating to a Duffing nonlinear oscillator subjected to combined stochastic and deterministic periodic loading, and to an oscillator with asymmetric nonlinearities and fractional derivative elements are considered for demonstrating the reliability of the technique. Juxtapositions with pertinent MCS data are included as well.

2. Preliminaries

2.1. Wiener path integral formalism

The equation of motion of a stochastically excited m–degree-of-freedom (m–DOF) structural system can be cast as a coupled system of second-order stochastic differential equations (SDEs) in the form

$$\boldsymbol{M}\ddot{\boldsymbol{x}}+\boldsymbol{C}\dot{\boldsymbol{x}}+\boldsymbol{K}\boldsymbol{x}+\boldsymbol{g}(\boldsymbol{x},\dot{\boldsymbol{x}},t)=\boldsymbol{w}(t), \tag{1}$$

where $\boldsymbol{x}$ denotes the displacement vector process $\left(\boldsymbol{x}=[x_1,\ldots,x_m]^T\right)$; $\boldsymbol{M}$, $\boldsymbol{C}$, $\boldsymbol{K}$ are the $m\times m$ mass, damping and stiffness matrices, respectively; and $\boldsymbol{g}(\cdot)$ represents a nonlinear vector function that can also account for possible dependence of the state of the system on its history. Further, $\boldsymbol{w}(t)$ is a white noise stochastic vector process with $\mathbb{E}[\boldsymbol{w}(t)]=0$ and $\mathbb{E}[\boldsymbol{w}(t)\boldsymbol{w}^T(t+\tau)]=\boldsymbol{S}_{\boldsymbol{w}}\delta(\tau)$, where $\boldsymbol{S}_{\boldsymbol{w}}\in\mathbb{R}^{m\times m}$ is a non-singular diagonal matrix.

In comparison to alternative derivations in the literature, a novel WPI formulation was developed by Mavromatis et al. [23] that circumvents the Markovian assumption for the system response process. In this regard, nonlinear systems with a history-dependent state, such as hysteretic structures or oscillators endowed with fractional derivative elements, can be treated in a direct manner. That is, without resorting to ad hoc modifications of the equations of motion pertaining, typically, to employing additional auxiliary filter equations and state variables (e.g., [25]).

Specifically, the probability of a path corresponding to an n-dimensional Wiener vector process with $\boldsymbol{W}(t_0)=\boldsymbol{W}_0$, $\boldsymbol{W}(t_f)=\boldsymbol{W}_f$ and $\Delta\boldsymbol{W}_l=\boldsymbol{W}_{l+1}-\boldsymbol{W}_l$ is given by (e.g., [26])

$$\mathcal{P}[\boldsymbol{W}(t)]=\lim_{\epsilon\to 0}\left\{\exp\left(-\frac{1}{2\epsilon}\sum_{l=0}^{L}\Delta\boldsymbol{W}_l^T\Delta\boldsymbol{W}_l\right)\times\prod_{l=0}^{L}\left[\sqrt{(2\pi\epsilon)^n}\right]^{-1}\prod_{j=1}^{n}\left[\prod_{l=1}^{L+1}\mathrm{d}W_{j,l}\right]\right\}, \tag{2}$$

where the time domain is discretized into $L+2$ points ϵ apart (with $L\to\infty$ as $\epsilon\to 0$), i.e., $t_i=t_0<\cdots<t_{L+1}=t_f$. Further, considering Eq. (2) and accounting for the probabilities of all possible paths that the Wiener process $\boldsymbol{W}$ can follow, the corresponding transition PDF is given as the limit of an L–dimensional integral in the form

$$p\left(\boldsymbol{W}_f,t_f|\boldsymbol{W}_i,t_i\right)=\lim_{\epsilon\to 0}\int_{-\infty}^{\infty}\cdots\int_{-\infty}^{\infty}\exp\left(-\frac{1}{2\epsilon}\sum_{l=0}^{L}\Delta\boldsymbol{W}_l^T\Delta\boldsymbol{W}_l\right)\times\prod_{l=0}^{L}\left[\sqrt{(2\pi\epsilon)^n}\right]^{-1}\prod_{j=1}^{n}\left[\prod_{l=1}^{L+1}\mathrm{d}W_{j,l}\right]. \tag{3}$$

Regarding the relation between the Wiener and the white noise processes, a unit intensity white noise process $\boldsymbol{w}(t)$, (i.e., $\boldsymbol{S}_{\boldsymbol{w}}=I$, where I is the identity matrix) can be defined as an infinitesimal jump of the Wiener process, i.e., $\boldsymbol{w}(t)\mathrm{d}t=\mathrm{d}\boldsymbol{W}$. Thus, it is often, informally, written as the time derivative of the Wiener process in the form $\boldsymbol{w}(t)=\frac{\mathrm{d}\boldsymbol{W}}{\mathrm{d}t}$; see also [27,28] for a more detailed discussion on the topic. Next, taking into account the relationship between the system response process $\boldsymbol{x}$ and the white noise process $\boldsymbol{w}$ described by Eq. (1), the transition PDF $p(\boldsymbol{x}_f,\dot{\boldsymbol{x}}_f,t_f|\boldsymbol{x}_i,\dot{\boldsymbol{x}}_i,t_i)$ is obtained by applying a functional change of variables to Eq. (3); see [23] for more details.

In this regard, denoting the set of all paths with initial state $\boldsymbol{x}_i$ at time t_i and final state $\boldsymbol{x}_f$ at time t_f by $C\{\boldsymbol{x}_f,\dot{\boldsymbol{x}}_f,t_f;\boldsymbol{x}_i,\dot{\boldsymbol{x}}_i,t_i\}$, the joint transition PDF $p(\boldsymbol{x}_f,\dot{\boldsymbol{x}}_f,t_f|\boldsymbol{x}_i,\dot{\boldsymbol{x}}_i,t_i)$ takes the form of a functional integral over $C\{\boldsymbol{x}_f,\dot{\boldsymbol{x}}_f,t_f;\boldsymbol{x}_i,\dot{\boldsymbol{x}}_i,t_i\}$; that is,

$$p(\boldsymbol{x}_f,\dot{\boldsymbol{x}}_f,t_f|\boldsymbol{x}_i,\dot{\boldsymbol{x}}_i,t_i)=\int_{C\{\boldsymbol{x}_f,\dot{\boldsymbol{x}}_f,t_f;\boldsymbol{x}_i,\dot{\boldsymbol{x}}_i,t_i\}}\exp\left(-S[\boldsymbol{x},\dot{\boldsymbol{x}},\ddot{\boldsymbol{x}}]\right)\mathcal{D}[\boldsymbol{x}(t)], \tag{4}$$

where

$$S[\boldsymbol{x},\dot{\boldsymbol{x}},\ddot{\boldsymbol{x}}]=\int_{t_i}^{t_f}\mathcal{L}[\boldsymbol{x},\dot{\boldsymbol{x}},\ddot{\boldsymbol{x}}]\mathrm{d}t \tag{5}$$

denotes the so-called (e.g., [26]) stochastic action. The Lagrangian functional $\mathcal{L}[\boldsymbol{x},\dot{\boldsymbol{x}},\ddot{\boldsymbol{x}}]$ in Eq. (5) takes the form

$$\mathcal{L}[\boldsymbol{x},\dot{\boldsymbol{x}},\ddot{\boldsymbol{x}}]=\frac{1}{2}\left[\boldsymbol{M}\ddot{\boldsymbol{x}}+\boldsymbol{C}\dot{\boldsymbol{x}}+\boldsymbol{K}\boldsymbol{x}+\boldsymbol{g}(\boldsymbol{x},\dot{\boldsymbol{x}},t)\right]^T\times\boldsymbol{S}_{\boldsymbol{w}}^{-1}\left[\boldsymbol{M}\ddot{\boldsymbol{x}}+\boldsymbol{C}\dot{\boldsymbol{x}}+\boldsymbol{K}\boldsymbol{x}+\boldsymbol{g}(\boldsymbol{x},\dot{\boldsymbol{x}},t)\right] \tag{6}$$

and the functional measure $\mathcal{D}[\boldsymbol{x}(t)]$ is given by the equation

$$\mathcal{D}[\boldsymbol{x}(t)]=\prod_{j=1}^{m}\mathcal{D}[\boldsymbol{x}_j(t)]=\prod_{j=1}^{m}\prod_{t=t_i}^{t_f}\frac{\mathrm{d}x_j(t)}{\sqrt{2\pi\left(\det\left[\boldsymbol{M}^{-1}\boldsymbol{S}_{\boldsymbol{w}}\left(\boldsymbol{M}^{-1}\right)^T\right]\right)^{1/m}\mathrm{d}t}}. \tag{7}$$

2.2. Most probable path approximation

It is noted that the analytical evaluation of the WPI of Eq. (4) is, in general, not feasible. Thus, alternative approaches are typically pursued in the literature for evaluating approximately Eq. (4), such as the most probable path approach (e.g., [26]). Note that the most probable path approximation has exhibited a quite high degree of accuracy in various diverse engineering mechanics applications (e.g., [17,18]).

Specifically, the largest contribution to the functional integral of Eq. (4) relates to the trajectory $\boldsymbol{x}_c(t)$ for which the stochastic action of Eq. (5) becomes as small as possible. This leads to the variational, functional minimization, problem

$$\underset{C\{\boldsymbol{x}_i,\dot{\boldsymbol{x}}_i,t_i;\boldsymbol{x}_f,\dot{\boldsymbol{x}}_f,t_f\}}{\text{minimize}}\quad S[\boldsymbol{x},\dot{\boldsymbol{x}},\ddot{\boldsymbol{x}}] \tag{8}$$

to be solved for $\boldsymbol{x}_c(t)$ in conjunction with the boundary conditions

$$[\boldsymbol{x}(t_i), \dot{\boldsymbol{x}}(t_i), \boldsymbol{x}(t_f), \dot{\boldsymbol{x}}(t_f)]^T = [\boldsymbol{x}_i, \dot{\boldsymbol{x}}_i, \boldsymbol{x}_f, \dot{\boldsymbol{x}}_f]^T. \tag{9}$$

Next, the functional integral of Eq. (4) is evaluated approximately as

$$p(\boldsymbol{x}_f, \dot{\boldsymbol{x}}_f, t_f | \boldsymbol{x}_i, \dot{\boldsymbol{x}}_i, t_i) = C \exp\left(-S[\boldsymbol{x}_c, \dot{\boldsymbol{x}}_c, \ddot{\boldsymbol{x}}_c]\right), \tag{10}$$

where C is a constant to be determined by the normalization condition

$$\int_{-\infty}^{\infty}\int_{-\infty}^{\infty} p(\boldsymbol{x}_f, \dot{\boldsymbol{x}}_f, t_f | \boldsymbol{x}_i, \dot{\boldsymbol{x}}_i, t_i) \mathrm{d}\boldsymbol{x}_f \mathrm{d}\dot{\boldsymbol{x}}_f = 1. \tag{11}$$

Notably, various methodologies can be employed for treating the optimization problem of Eq. (8) and for determining $\boldsymbol{x}_c(t)$. For instance, the most probable path $\boldsymbol{x}_c(t)$, being an extremal of $S[\boldsymbol{x}, \dot{\boldsymbol{x}}, \ddot{\boldsymbol{x}}]$, is determined by resorting to calculus of variations (e.g., [29]) and by enforcing the necessary condition that the first variation vanishes, i.e., $\delta S = 0$. This yields a system of Euler–Lagrange equations to be solved numerically for $\boldsymbol{x}_c(t)$ (e.g., [21]). Further, alternative approaches for obtaining the most probable path range from standard Rayleigh–Ritz solution treatments of Eq. (8) (e.g., [17,30]) to more recently developed techniques relying on computational algebraic geometry tools [31].

3. Mathematical formulation

As discussed in Section 2.2, the most probable path $\boldsymbol{x}_c(t)$, which is used for determining approximately the system response joint transition PDF via Eq. (10), is computed by solving a functional minimization problem in the form of Eq. (8) in conjunction with the boundary conditions of Eq. (9). Clearly, this BVP corresponds to a specific grid point of the response PDF domain. In fact, for a given time instant t_f, a standard brute-force numerical implementation of the technique (e.g., [19]) involves the discretization of the PDF effective domain into N^{2m} points, where N is the number of points in each dimension. Next, the evaluation of the PDF is performed point-wise on the discretized lattice. In other words, N^{2m} BVPs in the form of Eqs. (8) and (9) need to be solved numerically, inducing an exponential increase of the computational cost with the dimension m of the system.

To circumvent the aforementioned challenge, attention is directed in the following to the fact that, for a specific nonlinear system under consideration, the BVPs to be solved are independent of the grid point. In fact, only the boundary conditions change with different grid points, whereas the form of the problem remains unaltered. Remarkably, the BVPs corresponding to two neighboring grid points not only share the same equations, but also the boundary conditions differ only slightly. Thus, it is expected that their solutions, i.e., the most probable paths referring to the two grid points, are highly correlated. This unique aspect of the technique is explored further in the ensuing analysis, and it is shown that solution of a BVP and determination of the response PDF value at a specific grid point can be used for extrapolating and estimating efficiently, and accurately, the PDF values at neighboring points without the need for solving additional BVPs.

3.1. Relationship between the system response PDF estimates at two distinct points

Consider a point $(\boldsymbol{x}'_f, \dot{\boldsymbol{x}}'_f)$ in the response PDF domain that is related to point $(\boldsymbol{x}_f, \dot{\boldsymbol{x}}_f)$ in Eq. (9) as $(\boldsymbol{x}'_f, \dot{\boldsymbol{x}}'_f) = (\boldsymbol{x}_f + \Delta\boldsymbol{x}_f, \dot{\boldsymbol{x}}_f + \Delta\dot{\boldsymbol{x}}_f)$, where $(\Delta\boldsymbol{x}_f, \Delta\dot{\boldsymbol{x}}_f)$ denotes the difference between the two points. In this regard, referring to point $(\boldsymbol{x}'_f, \dot{\boldsymbol{x}}'_f)$, Eqs. (8) and (9) become

$$\underset{C\{\boldsymbol{x}_i, \dot{\boldsymbol{x}}_i, t_i; \boldsymbol{x}'_f, \dot{\boldsymbol{x}}'_f, t_f\}}{\text{minimize}} \quad S[\boldsymbol{x}, \dot{\boldsymbol{x}}, \ddot{\boldsymbol{x}}] \tag{12}$$

and

$$[\boldsymbol{x}(t_i), \dot{\boldsymbol{x}}(t_i), \boldsymbol{x}'(t_f), \dot{\boldsymbol{x}}'(t_f)]^T = [\boldsymbol{x}_i, \dot{\boldsymbol{x}}_i, \boldsymbol{x}'_f, \dot{\boldsymbol{x}}'_f]^T, \tag{13}$$

respectively. Next, the solution of Eqs. (12) and (13), which is the most probable path corresponding to initial conditions $(\boldsymbol{x}_i, \dot{\boldsymbol{x}}_i)$ and final conditions $(\boldsymbol{x}'_f, \dot{\boldsymbol{x}}'_f)$, is expressed as $\boldsymbol{x}'_c = \boldsymbol{x}_c + \Delta\boldsymbol{x}$, where $\Delta\boldsymbol{x}$ denotes a path to be determined. Further, substituting $\boldsymbol{x}'_c = \boldsymbol{x}_c + \Delta\boldsymbol{x}$ into the Lagrangian functional of Eq. (6) yields

$$\begin{aligned}\mathcal{L}[\boldsymbol{x}'_c, \dot{\boldsymbol{x}}'_c, \ddot{\boldsymbol{x}}'_c] = \frac{1}{2}\Big[&\boldsymbol{M}(\ddot{\boldsymbol{x}}_c + \Delta\ddot{\boldsymbol{x}}) + \boldsymbol{C}(\dot{\boldsymbol{x}}_c + \Delta\dot{\boldsymbol{x}}) + \\ &+ \boldsymbol{K}(\boldsymbol{x}_c + \Delta\boldsymbol{x}) + \boldsymbol{g}\left(\boldsymbol{x}_c + \Delta\boldsymbol{x}, \dot{\boldsymbol{x}}_c + \Delta\dot{\boldsymbol{x}}, t\right)\Big]^T \\ &\times \boldsymbol{S}_{\boldsymbol{w}}^{-1}\Big[\boldsymbol{M}(\ddot{\boldsymbol{x}}_c + \Delta\ddot{\boldsymbol{x}}) + \boldsymbol{C}(\dot{\boldsymbol{x}}_c + \Delta\dot{\boldsymbol{x}}) + \\ &+ \boldsymbol{K}(\boldsymbol{x}_c + \Delta\boldsymbol{x}) + \boldsymbol{g}\left(\boldsymbol{x}_c + \Delta\boldsymbol{x}, \dot{\boldsymbol{x}}_c + \Delta\dot{\boldsymbol{x}}, t\right)\Big].\end{aligned} \tag{14}$$

Eq. (14) is cast, equivalently, in the form

$$\begin{aligned}&\mathcal{L}[\boldsymbol{x}'_c, \dot{\boldsymbol{x}}'_c, \ddot{\boldsymbol{x}}'_c] = \\ &\frac{1}{2}\left[\left(\boldsymbol{A}(\boldsymbol{x}_c, \Delta\boldsymbol{x}) + \boldsymbol{B}_{\mathrm{lin}}(\Delta\boldsymbol{x})\right)^T \boldsymbol{S}_{\boldsymbol{w}}^{-1}\left(\boldsymbol{A}(\boldsymbol{x}_c, \Delta\boldsymbol{x}) + \boldsymbol{B}_{\mathrm{lin}}(\Delta\boldsymbol{x})\right)\right],\end{aligned} \tag{15}$$

where

$$\boldsymbol{A}(\boldsymbol{x}_c, \Delta\boldsymbol{x}) = \boldsymbol{M}\ddot{\boldsymbol{x}}_c + \boldsymbol{C}\dot{\boldsymbol{x}}_c + \boldsymbol{K}\boldsymbol{x}_c + \boldsymbol{g}\left(\boldsymbol{x}_c + \Delta\boldsymbol{x}, \dot{\boldsymbol{x}}_c + \Delta\dot{\boldsymbol{x}}, t\right), \tag{16}$$

and

$$\boldsymbol{B}_{\mathrm{lin}}(\Delta\boldsymbol{x}) = \boldsymbol{M}\Delta\ddot{\boldsymbol{x}} + \boldsymbol{C}\Delta\dot{\boldsymbol{x}} + \boldsymbol{K}\Delta\boldsymbol{x}. \tag{17}$$

Further, based on Eq. (10), the joint response PDF $p(\boldsymbol{x}'_f, \dot{\boldsymbol{x}}'_f, t_f | \boldsymbol{x}_i, \dot{\boldsymbol{x}}_i, t_i)$ is given by the equation

$$p(\boldsymbol{x}'_f, \dot{\boldsymbol{x}}'_f, t_f | \boldsymbol{x}_i, \dot{\boldsymbol{x}}_i, t_i) = C \exp\left(-S[\boldsymbol{x}'_c, \dot{\boldsymbol{x}}'_c, \ddot{\boldsymbol{x}}'_c]\right). \tag{18}$$

It is readily seen that Eq. (18) depends on $\boldsymbol{x}'_c = \boldsymbol{x}_c + \Delta\boldsymbol{x}$, where $\boldsymbol{x}_c$ is the most probable path corresponding to point $(\boldsymbol{x}_f, \dot{\boldsymbol{x}}_f)$ and $\Delta\boldsymbol{x}$ a path to be determined. In Section 3.2, it is shown that $\Delta\boldsymbol{x}$ can be evaluated approximately, in a closed form, at zero computational cost. Thus, once the $\boldsymbol{x}_c$ corresponding to the original point $(\boldsymbol{x}_f, \dot{\boldsymbol{x}}_f)$ has been determined, an extrapolation approach can be applied for obtaining the PDF values at neighboring points $(\boldsymbol{x}'_f, \dot{\boldsymbol{x}}'_f)$ without any additional computational effort.

3.2. Approximate analytical evaluation of the difference of the most probable paths corresponding to two neighboring points of the system response PDF domain

In the following, it is assumed that the two points of the system response PDF domain, $(\boldsymbol{x}_f, \dot{\boldsymbol{x}}_f)$ and $(\boldsymbol{x}'_f, \dot{\boldsymbol{x}}'_f)$, are sufficiently close to each other, and thus, their difference $(\Delta\boldsymbol{x}_f, \Delta\dot{\boldsymbol{x}}_f)$ is relatively small. Also, note that the two BVPs corresponding to $(\boldsymbol{x}_f, \dot{\boldsymbol{x}}_f)$ and $(\boldsymbol{x}'_f, \dot{\boldsymbol{x}}'_f)$ and described by Eqs. (8) and (9), and Eqs. (12) and (13), respectively, have identical equations with only slightly different boundary conditions. Thus, it is reasonable to assume that the term $\Delta\boldsymbol{x}$ is also relatively small. In other words, the solutions of the two BVPs, i.e., the two most probable paths $\boldsymbol{x}_c$ and $\boldsymbol{x}'_c$, corresponding to $(\boldsymbol{x}_f, \dot{\boldsymbol{x}}_f)$ and $(\boldsymbol{x}'_f, \dot{\boldsymbol{x}}'_f)$, respectively, are expected to differ only slightly.

Based on the preceding rationale, the approximation $\boldsymbol{g}\left(\boldsymbol{x}_c + \Delta\boldsymbol{x}, \dot{\boldsymbol{x}}_c + \Delta\dot{\boldsymbol{x}}, t\right) = \boldsymbol{g}\left(\boldsymbol{x}_c, \dot{\boldsymbol{x}}_c, t\right)$ is adopted next. In this regard, Eq. (16) becomes

$$\boldsymbol{A}(\boldsymbol{x}_c, \Delta\boldsymbol{x}) = \boldsymbol{A}(\boldsymbol{x}_c) = \boldsymbol{M}\ddot{\boldsymbol{x}}_c + \boldsymbol{C}\dot{\boldsymbol{x}}_c + \boldsymbol{K}\boldsymbol{x}_c + \boldsymbol{g}\left(\boldsymbol{x}_c, \dot{\boldsymbol{x}}_c, t\right) \tag{19}$$

and Eq. (15) takes the form

$$\mathcal{L}[\boldsymbol{x}'_c, \dot{\boldsymbol{x}}'_c, \ddot{\boldsymbol{x}}'_c] = \frac{1}{2}\left[\left(\boldsymbol{A}(\boldsymbol{x}_c) + \boldsymbol{B}_{\mathrm{lin}}(\Delta\boldsymbol{x})\right)^T \boldsymbol{S}_{\boldsymbol{w}}^{-1}\left(\boldsymbol{A}(\boldsymbol{x}_c) + \boldsymbol{B}_{\mathrm{lin}}(\Delta\boldsymbol{x})\right)\right]. \tag{20}$$

Further, consider the following general form for the diagonal matrix $\boldsymbol{S}_{\boldsymbol{w}}$; that is,

$$\boldsymbol{S}_{\boldsymbol{w}} = \begin{bmatrix} 2\pi S_1 & 0 & \cdots & 0 \\ 0 & 2\pi S_2 & \cdots & 0 \\ \vdots & \cdots & \ddots & \vdots \\ 0 & \cdots & 0 & 2\pi S_m \end{bmatrix}, \tag{21}$$

where S_i, $i = 1, \dots, m$ are positive constants denoting the intensities of the white noise processes. Next, taking into account Eq. (21), Eq. (20) is written, equivalently, as

$$\mathcal{L}[\boldsymbol{x}_c', \dot{\boldsymbol{x}}_c', \ddot{\boldsymbol{x}}_c'] = \frac{1}{2}\sum_{i=1}^{m} \frac{1}{2\pi S_i}(A_i + B_i)^2, \tag{22}$$

where

$$A_i = \sum_{j=1}^{m} m_{ij}\ddot{x}_{cj} + c_{ij}\dot{x}_{cj} + k_{ij}x_{cj} + g_j(\boldsymbol{x}_c, \dot{\boldsymbol{x}}_c, t) \tag{23}$$

and

$$B_i = \sum_{j=1}^{m} m_{ij}\Delta\ddot{x}_j + c_{ij}\Delta\dot{x}_j + k_{ij}\Delta x_j. \tag{24}$$

In Eqs. (23) and (24), m_{ij}, c_{ij}, k_{ij} denote the elements of the matrices $\boldsymbol{M}$, $\boldsymbol{C}$ and $\boldsymbol{K}$, respectively. Furthermore, employing the Cauchy–Schwarz inequality (e.g., [32]), Eq. (22) yields

$$\begin{aligned}\mathcal{L}[\boldsymbol{x}_c', \dot{\boldsymbol{x}}_c', \ddot{\boldsymbol{x}}_c'] &= \frac{1}{2}\sum_{i=1}^{m} \frac{1}{2\pi S_i}(A_i + B_i)^2 \\ &\le \frac{1}{2}\sum_{i=1}^{m} \frac{1}{2\pi S_i} 2(A_i^2 + B_i^2).\end{aligned} \tag{25}$$

Next, based on Eq. (25), $\mathcal{L}[\boldsymbol{x}_c', \dot{\boldsymbol{x}}_c', \ddot{\boldsymbol{x}}_c']$ is approximated by its upper bound as

$$\mathcal{L}_{\text{approx}}[\boldsymbol{x}_c', \dot{\boldsymbol{x}}_c', \ddot{\boldsymbol{x}}_c'] = \sum_{i=1}^{m} \frac{1}{2\pi S_i}(A_i^2 + B_i^2). \tag{26}$$

Equivalently, Eq. (26) can be expressed in a vectorial form as

$$\mathcal{L}_{\text{approx}}[\boldsymbol{x}_c', \dot{\boldsymbol{x}}_c', \ddot{\boldsymbol{x}}_c'] = \boldsymbol{A}^T(\boldsymbol{x}_c)\boldsymbol{S}_{\boldsymbol{w}}^{-1}\boldsymbol{A}(\boldsymbol{x}_c) + \boldsymbol{B}_{\text{lin}}^T(\Delta\boldsymbol{x})\boldsymbol{S}_{\boldsymbol{w}}^{-1}\boldsymbol{B}_{\text{lin}}(\Delta\boldsymbol{x}). \tag{27}$$

Obviously, decoupling has been achieved in Eq. (27), where the first term depends on $\boldsymbol{x}_c$ only, and the second term depends on $\Delta\boldsymbol{x}$ only. Further, considering the form of the Lagrangian of Eq. (6), Eq. (27) can be written, equivalently, as

$$\mathcal{L}_{\text{approx}}[\boldsymbol{x}_c', \dot{\boldsymbol{x}}_c', \ddot{\boldsymbol{x}}_c'] = 2\left(\mathcal{L}[\boldsymbol{x}_c, \dot{\boldsymbol{x}}_c, \ddot{\boldsymbol{x}}_c] + \mathcal{L}_{\text{lin}}[\Delta\boldsymbol{x}, \Delta\dot{\boldsymbol{x}}, \Delta\ddot{\boldsymbol{x}}]\right), \tag{28}$$

where

$$\mathcal{L}_{\text{lin}}(\Delta\boldsymbol{x}, \Delta\dot{\boldsymbol{x}}, \Delta\ddot{\boldsymbol{x}}) = \frac{1}{2}\boldsymbol{B}_{\text{lin}}^T(\Delta\boldsymbol{x})\boldsymbol{S}_{\boldsymbol{w}}^{-1}\boldsymbol{B}_{\text{lin}}(\Delta\boldsymbol{x}). \tag{29}$$

Next, substituting Eq. (28) into Eq. (5) yields

$$\mathcal{S}_{\text{approx}}[\boldsymbol{x}_c', \dot{\boldsymbol{x}}_c', \ddot{\boldsymbol{x}}_c'] = 2\left(\mathcal{S}[\boldsymbol{x}_c, \dot{\boldsymbol{x}}_c, \ddot{\boldsymbol{x}}_c] + \mathcal{S}_{\text{lin}}[\Delta\boldsymbol{x}, \Delta\dot{\boldsymbol{x}}, \Delta\ddot{\boldsymbol{x}}]\right), \tag{30}$$

where $\mathcal{S}_{\text{lin}}[\Delta\boldsymbol{x}, \Delta\dot{\boldsymbol{x}}, \Delta\ddot{\boldsymbol{x}}]$ is the stochastic action corresponding to the Lagrangian of Eq. (29). Further, following Section 3.1, $\boldsymbol{x}_c'$ is determined by solving the BVP of Eqs. (12) and (13), where $\mathcal{S}$ is approximated by $\mathcal{S}_{\text{approx}}$ of Eq. (30). Note, however, that in Eq. (30), the first term depends only on $\boldsymbol{x}_c$, which is considered to be a known function obtained by solving the BVP of Eqs. (8) and (9) corresponding to point $(\boldsymbol{x}_f, \dot{\boldsymbol{x}}_f)$. In this regard, $\mathcal{S}[\boldsymbol{x}_c, \dot{\boldsymbol{x}}_c, \ddot{\boldsymbol{x}}_c]$ is treated as a constant in the functional minimization problem, and thus, Eqs. (12) and (13) degenerate to

$$\underset{C\{0,0,t_i;\Delta\boldsymbol{x}_f,\Delta\dot{\boldsymbol{x}}_f,t_f\}}{\text{minimize}} \quad \mathcal{S}_{\text{lin}}[\Delta\boldsymbol{x}, \Delta\dot{\boldsymbol{x}}, \Delta\ddot{\boldsymbol{x}}] \tag{31}$$

and

$$[\Delta\boldsymbol{x}(t_i), \Delta\dot{\boldsymbol{x}}(t_i), \Delta\boldsymbol{x}(t_f), \Delta\dot{\boldsymbol{x}}(t_f)]^T = [\boldsymbol{0}, \boldsymbol{0}, \Delta\boldsymbol{x}_f, \Delta\dot{\boldsymbol{x}}_f]^T, \tag{32}$$

respectively. Next, resorting to the fundamental theorem of calculus of variations (e.g., [29]), the necessary condition is employed that the first variation of the functional of Eq. (31) vanishes, i.e., $\delta\mathcal{S}_{\text{lin}} = 0$. This yields the corresponding system of Euler–Lagrange equations for $j = 1, \dots, m$

$$\frac{\partial\mathcal{L}_{\text{lin}}}{\partial\Delta x_j} - \frac{\mathrm{d}}{\mathrm{d}t}\frac{\partial\mathcal{L}_{\text{lin}}}{\partial\Delta\dot{x}_j} + \frac{\mathrm{d}^2}{\mathrm{d}t^2}\frac{\partial\mathcal{L}_{\text{lin}}}{\partial\Delta\ddot{x}_j} = 0 \tag{33}$$

to be solved in conjunction with the boundary conditions of Eq. (32).

Notably, the form of the functional minimization problem of Eqs. (31) and (32), or, equivalently, of the associated Euler–Lagrange Eqs. (32) and (33), is identical to that corresponding to a linear oscillator under Gaussian white noise [33]. In fact, as shown in [33], Eqs. (32) and (33) are amenable to analytical solution treatment yielding

$$\Delta\boldsymbol{x} = C_1\boldsymbol{v}_1 e^{\lambda_1 t} + C_2\boldsymbol{v}_2 e^{\lambda_2 t} + \cdots + C_{4m}\boldsymbol{v}_{4m} e^{\lambda_{4m} t}, \tag{34}$$

where $[C_1, C_2, \dots, C_{4m}]^T$ is a vector containing $4m$ coefficients to be determined by enforcing the boundary conditions of Eq. (32) and $\{\boldsymbol{v}_1, \boldsymbol{v}_2, \dots, \boldsymbol{v}_{4m}\}$, $\{\lambda_1, \lambda_2, \dots, \lambda_{4m}\}$ are the eigenvectors and eigenvalues, respectively, of the associated eigenvalue problem. For more details on the derivation and the exact analytical expressions of the coefficients and of the eigenvalues and eigenvectors in Eq. (34), the interested reader is referred to [33].

In summary, the PDF value $p(\boldsymbol{x}_f', \dot{\boldsymbol{x}}_f', t_f|\boldsymbol{x}_i, \dot{\boldsymbol{x}}_i, t_i)$ at a point $(\boldsymbol{x}_f', \dot{\boldsymbol{x}}_f')$ sufficiently close to point $(\boldsymbol{x}_f, \dot{\boldsymbol{x}}_f)$ is evaluated herein by substituting $\boldsymbol{x}_c' = \boldsymbol{x}_c + \Delta\boldsymbol{x}$ in Eq. (18), where $\Delta\boldsymbol{x}$ is given by Eq. (34). From a computational cost perspective, it is highlighted that once the most probable path $\boldsymbol{x}_c(t)$ corresponding to the original point $(\boldsymbol{x}_f, \dot{\boldsymbol{x}}_f)$ has been determined, the herein developed extrapolation technique requires zero additional computational effort for obtaining the PDF values at neighboring points $(\boldsymbol{x}_f', \dot{\boldsymbol{x}}_f')$. Further, as shown in the numerical examples of Section 3.3, the accuracy degree of the technique is unaffected, practically, even for relatively large distances between points $(\boldsymbol{x}_f, \dot{\boldsymbol{x}}_f)$ and $(\boldsymbol{x}_f', \dot{\boldsymbol{x}}_f')$. The latter can be attributed, at least partly, to the fact that the expression for the response PDF in Eq. (18) is relatively insensitive to the exact form of $\boldsymbol{x}_c'$ as a function of time, and thus, an approximation in the form $\boldsymbol{x}_c' = \boldsymbol{x}_c + \Delta\boldsymbol{x}$, with $\Delta\boldsymbol{x}$ given by Eq. (34) is of satisfactory accuracy. This is due to the integral operator involved in the definition of the stochastic action $\mathcal{S}[\boldsymbol{x}_c', \dot{\boldsymbol{x}}_c', \ddot{\boldsymbol{x}}_c']$ that "averages" the time domain behavior of $\boldsymbol{x}_c'$.

3.3. Mechanization of the technique

Concisely stated, the mechanization of the technique comprises the following steps:

(a) For a given time instant t_f, discretize the domain of final states $\{\boldsymbol{x}_f, \dot{\boldsymbol{x}}_f\}$ into N^{2m} points, where N is the number of points in each dimension and $2m$ is the number of stochastic dimensions. N relates to the number of original points and is selected to be relatively small, e.g., $N \in [5, 15]$. Note that alternative, non-uniform and/or randomly generated, discretization meshes can be also used in principle.

(b) For each one of the N^{2m} points $\{\boldsymbol{x}_f, \dot{\boldsymbol{x}}_f\}$, determine the most probable path $\boldsymbol{x}_c(t)$ by solving numerically Eqs. (8) and (9).

(c) Consider the extrapolation domain of final states discretized into M^{2m} points, where M is the number of points in each dimension with $M \gg N$.

(d) For each one of the M^{2m} points $\{\boldsymbol{x}_f', \dot{\boldsymbol{x}}_f'\}$ in the extrapolation domain, determine its closest point $\{\boldsymbol{x}_f, \dot{\boldsymbol{x}}_f\}$ in the original domain.

(e) Evaluate the most probable path $\boldsymbol{x}_c'$ corresponding to point $\{\boldsymbol{x}_f', \dot{\boldsymbol{x}}_f'\}$ as $\boldsymbol{x}_c' = \boldsymbol{x}_c + \Delta\boldsymbol{x}$, where $\Delta\boldsymbol{x}$ is given by Eq. (34) in closed-form; see also Fig. 1 for a schematic.

(f) Obtain the system response transition PDF $p(\boldsymbol{x}_f', \dot{\boldsymbol{x}}_f', t_f|\boldsymbol{x}_i, \dot{\boldsymbol{x}}_i, t_i)$ by substituting $\boldsymbol{x}_c' = \boldsymbol{x}_c + \Delta\boldsymbol{x}$ into Eq. (18).

4. Numerical examples

4.1. Duffing nonlinear oscillator subjected both to stochastic loading and to a deterministic harmonic excitation component

Consider a single-DOF Duffing nonlinear oscillator subjected to combined loading. Its equation of motion is given by

$$m\ddot{x} + c\dot{x} + kx + \epsilon x^3 = w(t) + F\cos(\omega t). \tag{35}$$

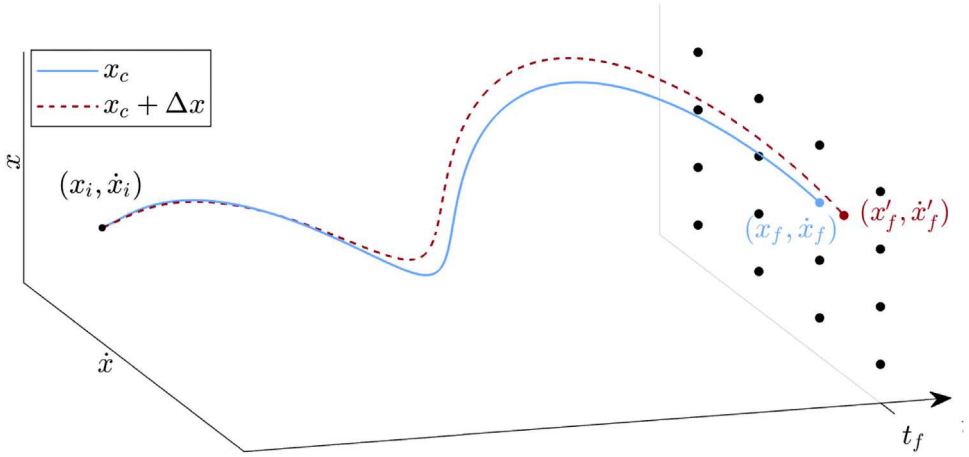

Fig. 1. Extrapolation approach shown for a generic single-DOF oscillator: Original discretization mesh and a representative most probable path $\boldsymbol{x}_c$ corresponding to point $(\boldsymbol{x}_f, \dot{\boldsymbol{x}}_f)$ (blue); representative extrapolated most probable path at point $(\boldsymbol{x}'_f, \dot{\boldsymbol{x}}'_f)$ evaluated as $\boldsymbol{x}'_c = \boldsymbol{x}_c + \boldsymbol{\Delta x}$ (red). (For interpretation of the references to color in this figure legend, the reader is referred to the web version of this article.)

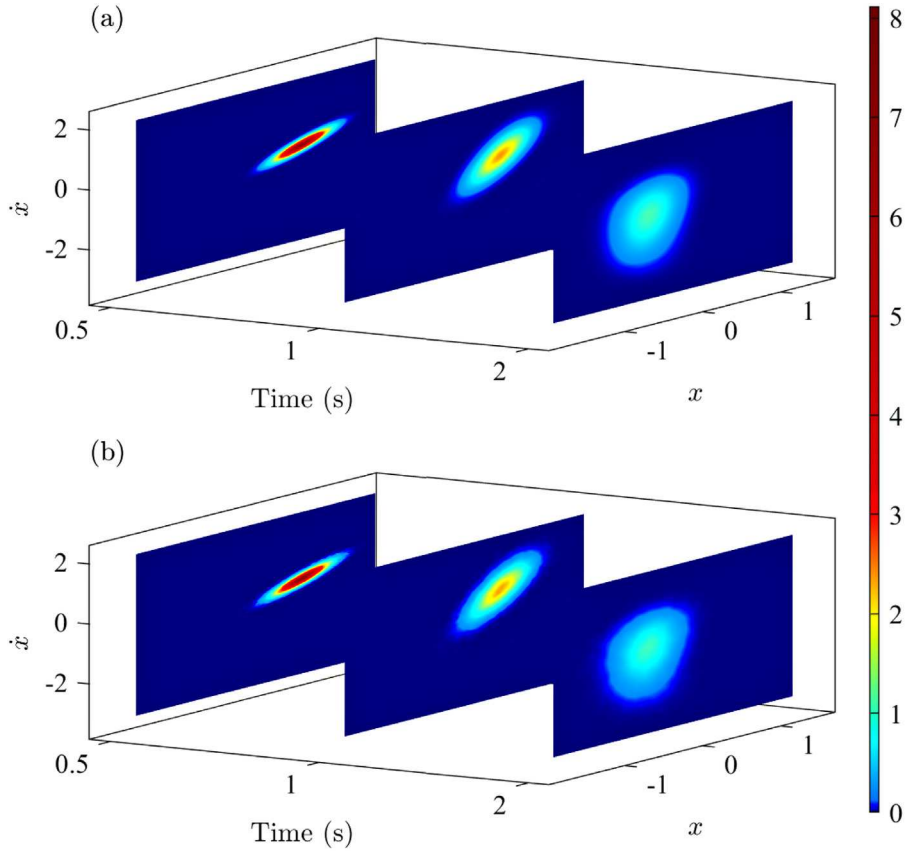

Fig. 2. Joint response PDF at indicative time instants $t_f = 0.5$, 1 and 2 s corresponding to a Duffing nonlinear oscillator subjected both to stochastic loading and to a deterministic harmonic excitation component: (a) results obtained by the WPI technique at $N^2 = 7^2$ points and extrapolated at $N^2 = 201^2$ points; (b) comparison with MCS data (100,000 realizations).

Obviously, the applied excitation comprises a white noise ($w(t)$) and a deterministic harmonic ($F\cos(\omega t)$) components. In passing, note recent extensions of alternative standard approximate techniques, such as stochastic averaging and statistical linearization, to account for such challenging cases of combined stochastic and deterministic periodic loading (e.g., [34–37]). In this regard, it is shown herein that such types of combined loading, for which the purely stochastic excitation can be construed as a special case, can be treated by the WPI technique in a straightforward manner without the need for any modifications of the original formulation. Indeed, Eq. (35) can be written, equivalently, in the form of Eq. (1) with $\boldsymbol{g}(x, \dot{x}, t) = \epsilon x^3 - F\cos(\omega t)$ and parameter values $m = 1, c = 0.5, k = 1, \epsilon = 1, F = 1.5, \omega = 2, S_0 = 0.05$.

Next, for three arbitrarily selected time instants $t_f = 0.5$, 1, 2s, the joint response PDF $p(x_f, \dot{x}_f, t_f|0, 0, 0)$ is evaluated at $N^2 = 7^2$ points based on the WPI technique. Further, the herein developed extrapolation approach is employed for estimating the PDF values at a grid of $N^2 = 201^2$ points spanning the entire PDF domain. The results are plotted in Fig. 2(a) and compared with MCS-based estimates (100,000 realizations) in Fig. 2(b). The MCS data are obtained by

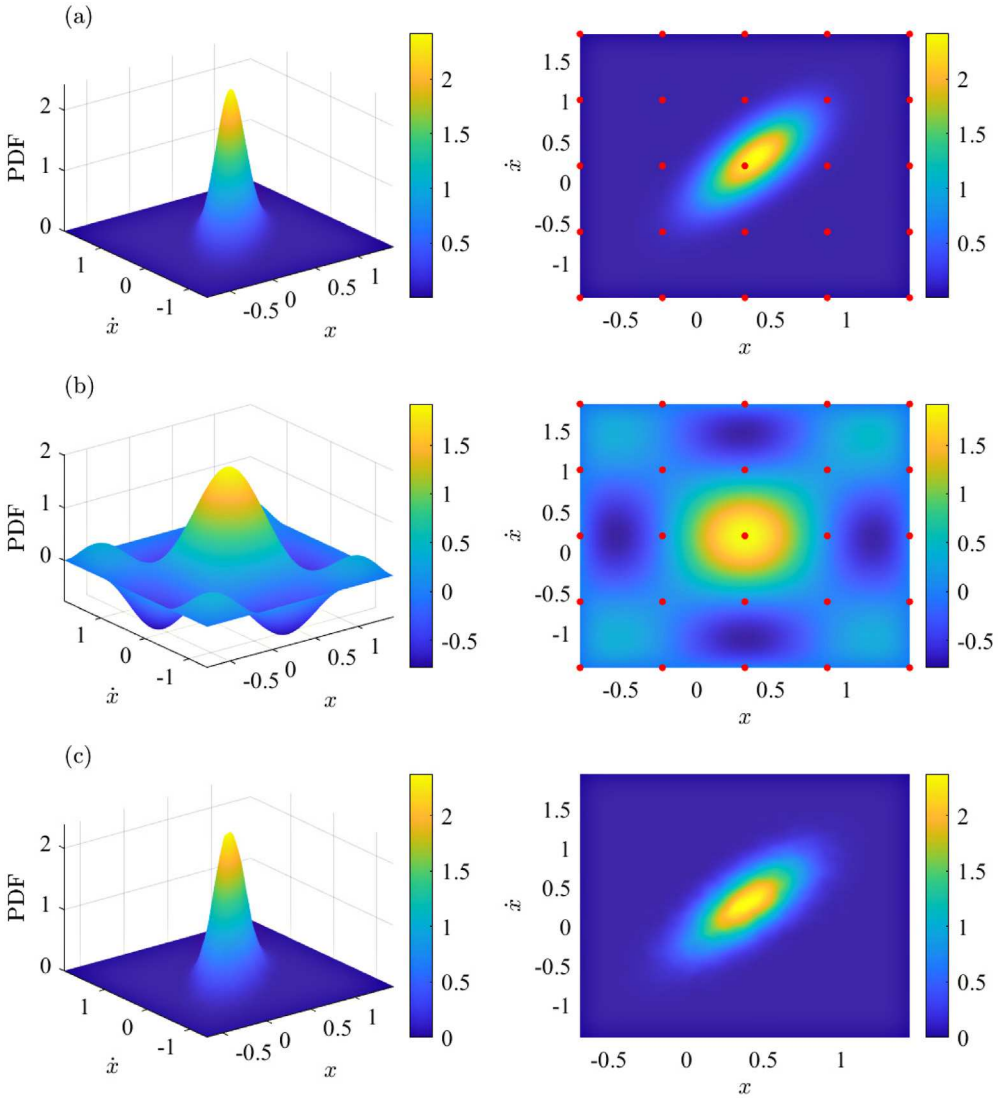

Fig. 3. Joint response PDF at an indicative time instant $t_f = 1s$ corresponding to a Duffing nonlinear oscillator subjected both to stochastic loading and to a deterministic harmonic excitation component: (a) results obtained by the WPI technique at $N^2 = 5^2$ points and extrapolated at $N^2 = 201^2$ points; (b) results based on a splines extrapolation scheme using the same original mesh of $N^2 = 5^2$ points as in (a); (c) comparison with MCS data (100,000 realizations). (For interpretation of the references to color in this figure legend, the reader is referred to the web version of this article.)

numerically solving the equation of motion based on a standard Runge–Kutta integration scheme (e.g., [38]) and by conducting a statistical analysis on the response time-histories. Further, to highlight the quite high degree of accuracy, even for relatively large distances between the original and the extrapolated points, the WPI-based joint response PDF at $t_f = 1s$ is shown in Fig. 3(a) in conjunction with the original mesh of $N^2 = 5^2$ points (red dots). This is compared, indicatively, with a purely data-based splines extrapolation scheme (e.g., [39]) that provides the PDF estimate shown in Fig. 3(b). Obviously, due to the quite small number of original mesh points, the splines-based scheme fails to capture even the basic shape of the PDF compared with the MCS-based estimate of Fig. 3(c). Also, the splines-based estimates violate the property of the PDF being non-negative.

In Fig. 4, the y-axis shows the mean square error of the PDF estimates compared with the MCS-based solution (100,000 realizations). The x-axis shows the computation time required for obtaining the PDF estimates. Clearly, for a given degree of accuracy, the proposed extrapolation approach is several orders of magnitude more efficient than both a brute-force implementation of the WPI technique and a standard MCS solution scheme.

4.2. Oscillator with asymmetric nonlinearities and fractional derivative elements

Consider next a single-DOF oscillator with asymmetric nonlinearities and fractional derivative elements. Its equation of motion is given by

$$m\ddot{x} + c\,{}_{t_i}^{C}D_t^a x + k(x + \epsilon x^2) = w(t) \tag{36}$$

where ${}_{t_i}^{C}D_t^a x$ represents the left Caputo fractional derivative of order a defined as

$${}_{t_i}^{C}D_t^a x(t) = \frac{1}{\Gamma(1-a)} \int_{t_i}^{t} \frac{\dot{x}(\tau)}{(t-\tau)^a} \mathrm{d}\tau, \tag{37}$$

with $\Gamma(\cdot)$ denoting the Gamma function; and $0 < a < 1$. Eq. (36) can be written, equivalently, in the form of Eq. (1) with $g(x, \dot{x}, t) = -c\dot{x} + c\,{}_{t_i}^{C}D_t^a x + \epsilon k x^2$. The selected parameter values are $m = 1, c = 0.6, k = 1, \epsilon = 0.5, \alpha = 0.5$ and $S_0 = 0.05$. Next, the joint response PDF $p(x_f, \dot{x}_f, t_f | 0, 0, 0)$ is evaluated based on the WPI technique by employing a Rayleigh–Ritz scheme for solving the BVP of Eqs. (8) and (9) (e.g., [22]).

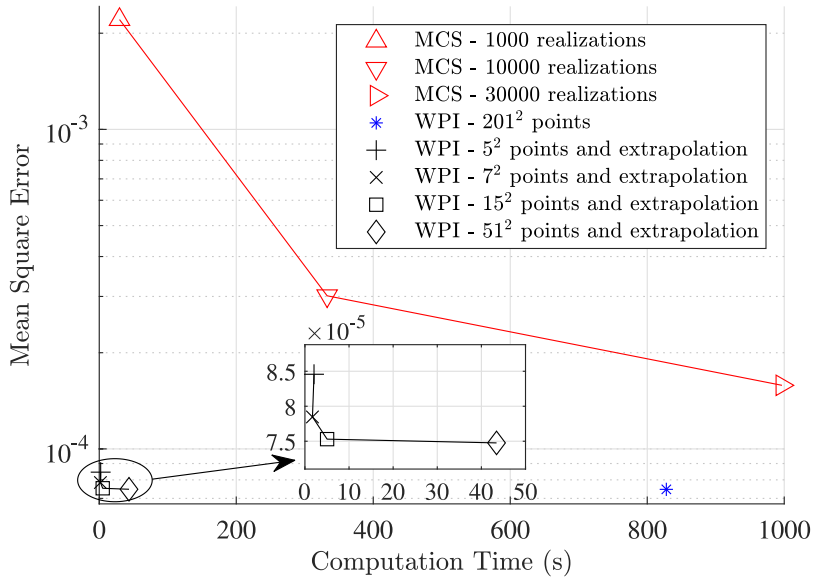

Fig. 4. Comparisons in terms of accuracy and computational cost between the standard MCS, the brute-force implementation of the WPI technique, and the efficient WPI technique based on extrapolation: mean square error and associated computation time for estimating the joint response PDF at an indicative time instant $t_f = 1s$ corresponding to a single-DOF Duffing nonlinear oscillator subjected both to stochastic loading and to a deterministic harmonic excitation component.

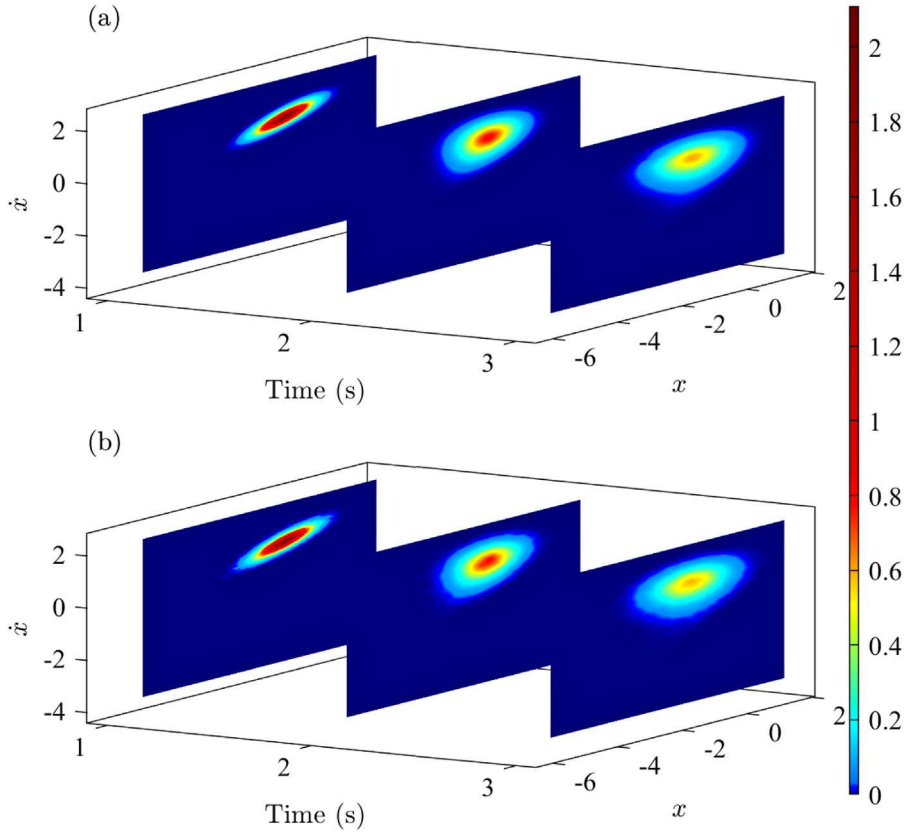

Fig. 5. Joint response PDF at indicative time instants $t_f = 1$, 2 and 3 s corresponding to an oscillator with asymmetric nonlinearities and fractional derivative elements: (a) results obtained by the WPI technique at $N^2 = 9^2$ points and extrapolated at $N^2 = 201^2$ points; (b) comparison with MCS data (100,000 realizations).

In passing, it is worth noting that the response of the oscillator in Eq. (36) cannot, strictly speaking, reach stationarity. This is due to the fact that escape from the corresponding potential energy well is possible if the displacement exceeds a critical level. Such an escape is followed, typically, by an unbounded response behavior. In the following numerical results, such an escape event has practically zero probability of occurrence for the selected parameter values and final time instants; see also section 5.3.6 in the book by Roberts and Spanos [10] for a relevant discussion.

Further, the herein-developed technique is used for evaluating the PDF values at an original mesh of $N^2 = 9^2$ points, and for extrapolating at a grid of $N^2 = 201^2$ points over the PDF domain. The results are plotted for three arbitrary time instants $t_f = 1$, 2, 3s in Fig. 5(a) and compared with MCS-based estimates (100,000 realizations) in Fig. 5(b)

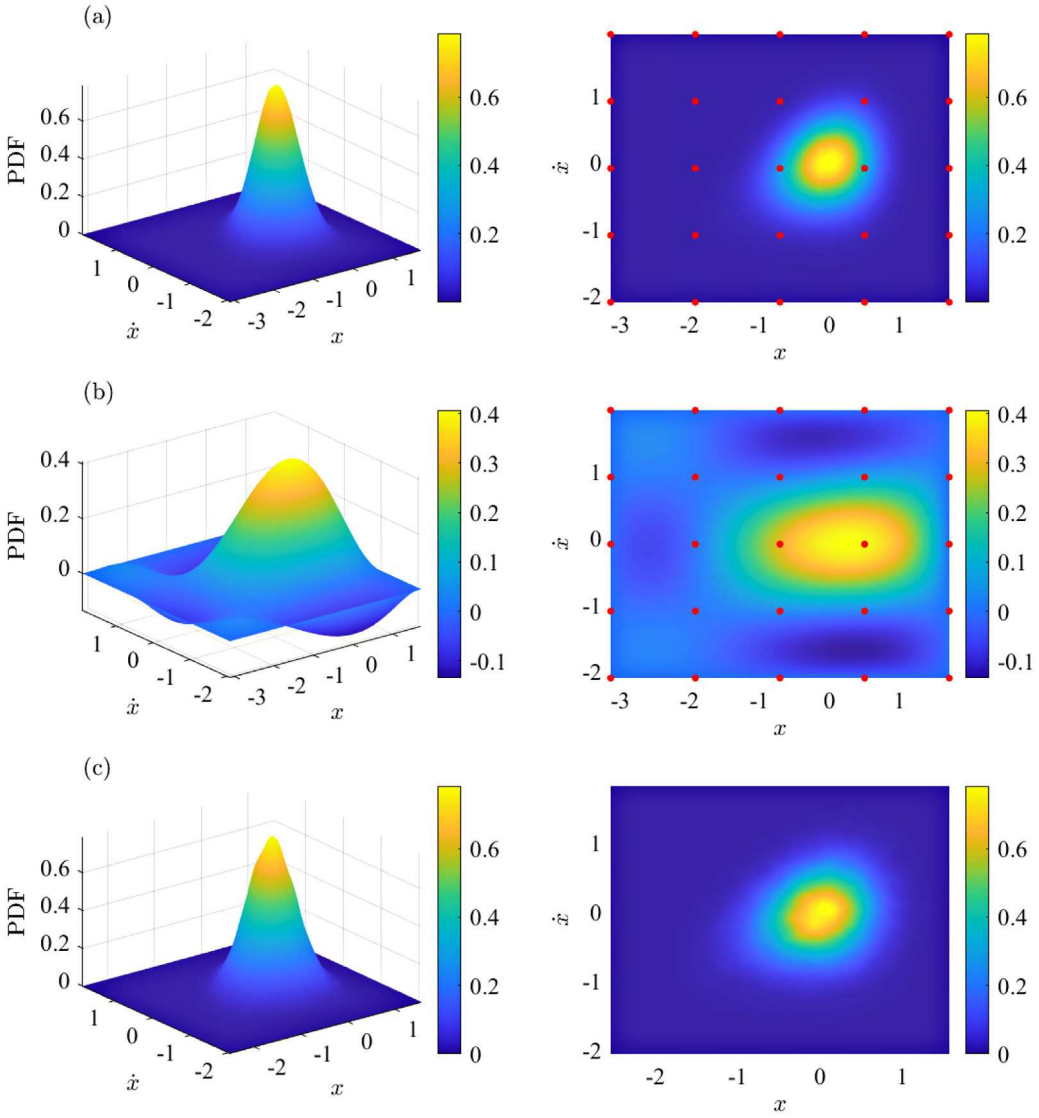

Fig. 6. Joint response PDF at an indicative time instant $t_f = 2s$ corresponding to an oscillator with asymmetric nonlinearities and fractional derivative elements: (a) results obtained by the WPI technique at $N^2 = 5^2$ points and extrapolated at $N^2 = 201^2$ points; (b) results based on a splines extrapolation scheme using the same original mesh of $N^2 = 5^2$ points as in (a); (c) comparison with MCS data (100,000 realizations). (For interpretation of the references to color in this figure legend, the reader is referred to the web version of this article.)

demonstrating a quite high degree of accuracy. For the MCS analyses, the $L1$ algorithm (e.g., [40]) has been used for integrating numerically Eq. (36) and for determining response realizations. Furthermore, the WPI-based PDF estimate for $t_f = 2s$ is plotted in Fig. 6(a) in conjunction with the original mesh of $N^2 = 5^2$ points (red dots). In Fig. 6(b), the splines-based PDF estimate is shown, obtained by using the same original mesh of $N^2 = 5^2$ points. Comparisons with the MCS-based estimate in Fig. 6(c) demonstrate, similarly to the example of Section 4.1, a quite low accuracy degree exhibited by the purely data-based splines extrapolation scheme (e.g., [39]).

Lastly, similarly to Fig. 6, in Fig. 7 the mean square error (y-axis) of the PDF estimates is plotted as a function of the computation time (x-axis) required for determining the PDF. For a given degree of accuracy, it is readily seen that the developed extrapolation approach vastly outperforms the standard MCS scheme in terms of efficiency.

5. Concluding remarks

A novel extrapolation approach has been developed in this paper that drastically reduces the computational cost associated with the WPI technique without, practically, affecting the exhibited accuracy. Specifically, the WPI technique for determining the stochastic response of diverse nonlinear dynamical systems relies on a variational formulation that leads to a functional minimization problem. This takes the form of a deterministic BVP to be solved for the most probable path, which is used for determining approximately the system response joint transition PDF. The BVP corresponds to a specific grid point of the response PDF effective domain. Remarkably, the BVPs corresponding to two neighboring grid points not only share the same equations, but also the boundary conditions differ only slightly. This unique aspect of the technique has been exploited herein and it has been shown that solution of a BVP and determination of the response PDF value at a specific grid point can be used for extrapolating and estimating efficiently, and accurately, the PDF values at neighboring points without the need for solving additional BVPs. In fact, the developed extrapolation approach has exhibited a quite high degree of accuracy even for relatively large distances between the original and the extrapolated points. Two numerical examples relating to a Duffing nonlinear oscillator subjected to combined stochastic and deterministic periodic loading, and to an oscillator with asymmetric nonlinearities and fractional derivative elements

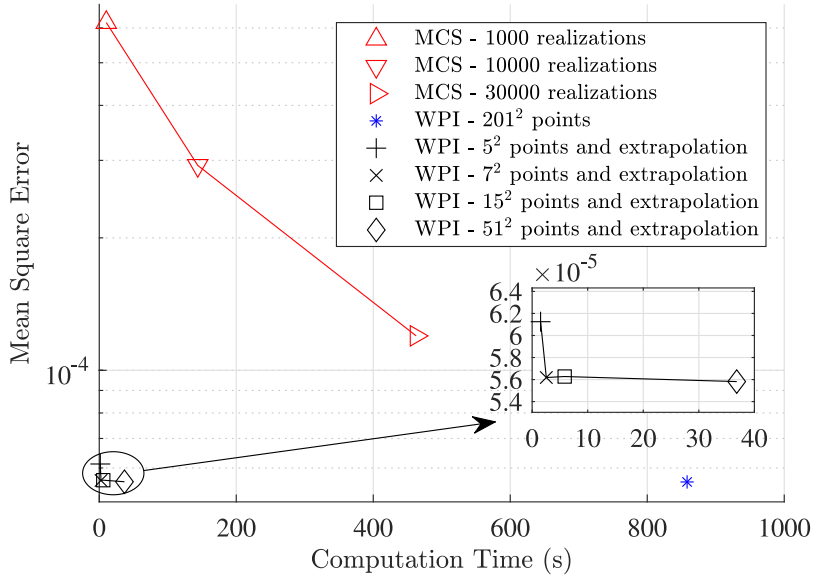

Fig. 7. Comparisons in terms of accuracy and computational cost between the standard MCS, the brute-force implementation of the WPI technique, and the efficient WPI technique based on extrapolation: mean square error and associated computation time for estimating the joint response PDF at an indicative time instant $t_f = 1s$ corresponding to a stochastically excited oscillator with asymmetric nonlinearities and fractional derivative elements.

have been considered for assessing the performance of the developed approach. It has been shown that, for a given degree of accuracy, the extrapolation approach is several orders of magnitude more efficient than both a brute-force implementation of the WPI technique and a standard MCS solution scheme.

CRediT authorship contribution statement

Ilias G. Mavromatis: Conceptualization, Methodology, Software, Writing – original draft, Writing – review & editing. **Ioannis A. Kougioumtzoglou:** Conceptualization, Funding acquisition, Methodology, Supervision, Writing – review & editing. **Pol D. Spanos:** Conceptualization, Writing – review & editing.

Declaration of competing interest

The authors declare that they have no known competing financial interests or personal relationships that could have appeared to influence the work reported in this paper.

Data availability

Data will be made available on request.

Acknowledgments

I. A. Kougioumtzoglou gratefully acknowledges the support through his CAREER award by the CMMI Division of the National Science Foundation, United States (Award No. 1748537).

References

[1] Y.K. Lin, Probabilistic Theory of Structural Dynamics, McGraw-Hill, 1967.
[2] N.C. Nigam, Introduction to Random Vibrations, The MIT Press, Cambridge, 1983.
[3] I. Elishakoff, Probabilistic Theory of Structures, second ed., Dover Publications, 1999.
[4] R.G. Ghanem, P.D. Spanos, Stochastic Finite Elements: A Spectral Approach, Dover Publications, 2003.
[5] L.D. Lutes, S. Sarkani, Random Vibrations: Analysis of Structural and Mechanical Systems, Elsevier-Butterworth-Heinemannier, 2004.
[6] M.F. Wehner, W.G. Wolfer, Numerical evaluation of path-integral solutions to Fokker–Planck equations, Phys. Rev. A 27 (5) (1983) 2663–2670, http://dx.doi.org/10.1103/PhysRevA.27.2663.
[7] A. Naess, J.M. Johnsen, Response statistics of nonlinear, compliant offshore structures by the path integral solution method, Probab. Eng. Mech. 8 (2) (1993) 91–106, http://dx.doi.org/10.1016/0266-8920(93)90003-E.
[8] H. Risken, The Fokker–Planck Equation: Methods of Solution and Applications, Springer-Verlag, Berlin, Heidelberg, 1984, http://dx.doi.org/10.1007/978-3-642-61544-3.
[9] J. Li, J. Chen, Stochastic Dynamics of Structures, John Wiley & Sons, Ltd, Chichester, UK, 2009, http://dx.doi.org/10.1002/9780470824269.
[10] J.B. Roberts, P.D. Spanos, Random Vibration and Statistical Linearization, Dover Publications, 2003.
[11] L. Socha, Linearization Methods for Stochastic Dynamic Systems, Vol. 730, Springer, Berlin, Heidelberg, 2007.
[12] M. Grigoriu, Applied Non-Gaussian Processes: Examples, Theory, Simulation, Linear Random Vibration, and Matlab Solutions, Prentice Hall, 1995.
[13] M. Shinozuka, G. Deodatis, Simulation of multi-dimensional Gaussian stochastic fields by spectral representation, Appl. Mech. Rev. 49 (1996) 29–53, http://dx.doi.org/10.1115/1.3101883.
[14] P.D. Spanos, B.A. Zeldin, Monte Carlo treatment of random fields: A broad perspective, Appl. Mech. Rev. 51 (1998) 219–237, http://dx.doi.org/10.1115/1.3098999.
[15] I.A. Kougioumtzoglou, Harmonic Wavelets Procedures and Wiener Path Integral Methods for Response Determination and Reliability Assessment of Nonlinear Systems/structures (Ph.D. thesis), Rice University, 2011.
[16] I.A. Kougioumtzoglou, P.D. Spanos, An analytical Wiener path integral technique for non-stationary response determination of nonlinear oscillators, Probab. Eng. Mech. 28 (2012) 125–131, http://dx.doi.org/10.1016/j.probengmech.2011.08.022.
[17] I.A. Kougioumtzoglou, A Wiener path integral solution treatment and effective material properties of a class of one-dimensional stochastic mechanics problems, J. Eng. Mech. 143 (6) (2017) 1–12, http://dx.doi.org/10.1061/(ASCE)EM.1943-7889.0001211.
[18] I. Petromichelakis, A.F. Psaros, I.A. Kougioumtzoglou, Stochastic response determination and optimization of a class of nonlinear electromechanical energy harvesters: A Wiener path integral approach, Probab. Eng. Mech. 53 (2018) 116–125, http://dx.doi.org/10.1016/j.probengmech.2018.06.004.
[19] A.F. Psaros, O. Brudastova, G. Malara, I.A. Kougioumtzoglou, Wiener Path Integral based response determination of nonlinear systems subject to non-white, non-Gaussian, and non-stationary stochastic excitation, J. Sound Vib. 433 (2018) 314–333, http://dx.doi.org/10.1016/j.jsv.2018.07.013.
[20] I. Petromichelakis, I.A. Kougioumtzoglou, Addressing the curse of dimensionality in stochastic dynamics: A Wiener path integral variational formulation with free boundaries, Proc. R. Soc. A 476 (2243) (2020) http://dx.doi.org/10.1098/rspa.2020.0385.
[21] A.F. Psaros, I.A. Kougioumtzoglou, Functional series expansions and quadratic approximations for enhancing the accuracy of the Wiener path integral technique, J. Eng. Mech. 146 (7) (2020) 04020065, http://dx.doi.org/10.1061/(asce)em.1943-7889.0001793.

[22] A. Di Matteo, I.A. Kougioumtzoglou, A. Pirrotta, P.D. Spanos, M. Di Paola, Stochastic response determination of nonlinear oscillators with fractional derivatives elements via the Wiener path integral, Probab. Eng. Mech. 38 (2014) 127–135, http://dx.doi.org/10.1016/j.probengmech.2014.07.001.

[23] I.G. Mavromatis, A.F. Psaros, I.A. Kougioumtzoglou, A Wiener path integral formalism for treating nonlinear systems with non-Markovian response processes, J. Eng. Mech. 149 (1) (2023) 1–11, http://dx.doi.org/10.1061/JENMDT.EMENG-6873.

[24] I.G. Mavromatis, I.A. Kougioumtzoglou, A reduced-order Wiener path integral formalism for determining the stochastic response of nonlinear systems with fractional derivative elements, ASCE-ASME J. Risk Uncertain Engrgy Syst. B Mech, Engrgy 9 (3) (2023) 1–9, http://dx.doi.org/10.1115/1.4056902.

[25] Y. Zhang, I.A. Kougioumtzoglou, F. Kong, A Wiener path integral technique for determining the stochastic response of nonlinear oscillators with fractional derivative elements: A constrained variational formulation with free boundaries, Probab. Eng. Mech. 71 (2023) 103410, http://dx.doi.org/10.1016/j.probengmech.2022.103410.

[26] M. Chaichian, A. Demichev, Path Integrals in Physics, Vol. 1, IOP Publishing Ltd, 2001, http://dx.doi.org/10.1887/0750307137.

[27] C. Gardiner, Handbook of Stochastic Methods for Physics, Chemistry, and the Natural Sciences, third ed., Springer-Verlag, 1985.

[28] B. Øksendal, Stochastic Differential Equations, fifth ed., in: Universitext, Springer, Berlin, Heidelberg, 2003, http://dx.doi.org/10.1007/978-3-642-14394-6.

[29] I.M. Gelfand, S.V. Fomin, The Calculus of Variations, Prentice Hall, 1963.

[30] I. Petromichelakis, A.F. Psaros, I.A. Kougioumtzoglou, Stochastic response determination of nonlinear structural systems with singular diffusion matrices: A Wiener path integral variational formulation with constraints, Probab. Eng. Mech. 60 (2020) 103044, http://dx.doi.org/10.1016/j.probengmech.2020.103044.

[31] I. Petromichelakis, R.M. Bosse, I.A. Kougioumtzoglou, A.T. Beck, Wiener path integral most probable path determination: A computational algebraic geometry solution treatment, Mech. Syst. Signal Process. 153 (2021) 107534, http://dx.doi.org/10.1016/j.ymssp.2020.107534.

[32] J.M. Steele, The Cauchy-Schwarz Master Class: An Introduction to the Art of Mathematical Inequalities, Cambridge University Press, 2004, http://dx.doi.org/10.1017/CBO9780511817106.

[33] A.F. Psaros, Y. Zhao, I.A. Kougioumtzoglou, An exact closed-form solution for linear multi-degree-of-freedom systems under Gaussian white noise via the Wiener path integral technique, Probab. Eng. Mech. 60 (2020) 103040, http://dx.doi.org/10.1016/j.probengmech.2020.103040.

[34] R. Haiwu, X. Wei, M. Guang, F. Tong, Response of a Duffing oscillator to combined deterministic harmonic and random excitation, J. Sound Vib. 242 (2) (2001) 362–368, http://dx.doi.org/10.1006/jsvi.2000.3329.

[35] N. Anh, N. Hieu, The Duffing oscillator under combined periodic and random excitations, Probab. Eng. Mech. 30 (2012) 27–36, http://dx.doi.org/10.1016/j.probengmech.2012.02.004.

[36] P.D. Spanos, Y. Zhang, F. Kong, Formulation of statistical linearization for M-D-O-F systems subject to combined periodic and stochastic excitations, J. Appl. Mech. 86 (10) (2019) 1–8, http://dx.doi.org/10.1115/1.4044087.

[37] Y. Zhang, P.D. Spanos, A linearization scheme for vibrations due to combined deterministic and stochastic loads, Probab. Eng. Mech. 60 (January) (2020) 103028, http://dx.doi.org/10.1016/j.probengmech.2020.103028.

[38] L.F. Shampine, M.W. Reichelt, The MATLAB ode suite, SIAM J. Sci. Comput. 18 (1) (1997) 1–22, http://dx.doi.org/10.1137/S1064827594276424.

[39] K. Atkinson, An Introduction to Numerical Analysis, second ed., John Wiley & Sons, Ltd, 1991.

[40] C.G. Koh, J.M. Kelly, Application of fractional derivatives to seismic analysis of base-isolated models, Earthq. Eng. Struct. Dyn. 19 (2) (1990) 229–241, http://dx.doi.org/10.1002/eqe.4290190207.